

Visibility-based hypothesis testing using higher-order optical interference

Michał Jachura^{1*}, Michał Lipka¹, Marcin Jarzyna², Wojciech Wasilewski¹, Konrad Banaszek^{1,2}

¹*Faculty of Physics, University of Warsaw, ul. Pasteura 5, 02-093 Warszawa*

²*Centre of New Technologies, University of Warsaw, ul. Banacha 2c, 02-097 Warszawa and*

**Corresponding author: michal.jachura@fuw.edu.pl*

Many quantum information protocols rely on optical interference to compare datasets with efficiency or security unattainable by classical means. Standard implementations exploit first-order coherence between signals whose preparation requires a shared phase reference. Here, we analyze and experimentally demonstrate binary discrimination of visibility hypotheses based on higher-order interference for optical signals with a random relative phase. This provides a robust protocol implementation primitive when a phase lock is unavailable or impractical. With the primitive cost quantified by the total detected optical energy, optimal operation is typically reached in the few-photon regime requiring photon number resolving capability.

Optical systems, in addition to being the workhorse of modern telecommunication, provide a natural platform to implement quantum-enhanced protocols for information transfer and processing between distant parties. Quantum strategies can provide authentication or reduce the communication complexity of certain tasks, in which large distributed datasets need to be processed to infer a relatively small amount of information [1, 2]. Examples include quantum digital signatures [3] and quantum fingerprinting [4]. These protocols share a primitive which consists in imprinting the input data onto the modal structure of transmitted fields, e.g. in the form of phase patterns, and interfering the received signals. Different hypotheses, e.g. the instances of identical and unequal inputs, are mapped onto distinct ranges of the interference visibility, which can therefore serve as the basis for hypothesis testing. Strikingly, optical signals sufficient to realize the quantum scheme may not have the capacity to carry information necessary to implement the classical protocols with the matching confidence level. This enhancement, stemming from the interplay between wave and particle properties of light exploited in quantum protocols, can advantageously change the scaling of resources required to perform the task as well as ensure security.

As recently pointed out [5, 6] and demonstrated experimentally [7–10], the protocol primitive described above can be realized efficiently with coherent light beams and first-order interference. This implementation uses laser light sources and is robust against attenuation introduced by optical channels transmitting the signals, but it requires phase stability between the sending parties. In certain scenarios a shared phase reference may be unavailable or very difficult to furnish. An alternative may be to resort to Hong-Ou-Mandel interference between single photons which has been exploited in proof-of-principle demonstrations of quantum communication complexity protocols [11, 12]. However, single

photon sources with characteristics needed for scalable implementation, e.g. long coherence times, may not be readily available. Crucially, single photon realizations are susceptible to losses: useful information is obtained only from events when both the photons are received in the same measurement run. Without quantum memories, the rate of such events exhibits unfavorable, quadratic scaling with the channel transmission. The same impairment would affect the realization based on weak classical states with a random global phase [13].

In this paper we present a strategy to carry out optical hypothesis testing based on the visibility of higher-order interference between classical fields with random relative phase. This approach concurrently benefits from conventional optical signal generation techniques, removes the need for a shared phase reference, and ensures robustness against channel attenuation. The performance is characterized using average error probability, whose asymptotic behavior is investigated with the help of a refined Chernoff bound [14, 15]. Interestingly, we show that when the protocol cost is quantified in terms of the total transmitted optical energy, the optimal strategy is to realize multiple repetitions of the interference visibility measurement in the few-photon regime with a determination of the complete photocount statistics. This makes photon number resolving (PNR) detection an essential ingredient of the presented approach.

Let us start by considering interference between two coherent optical signals with overall optical energy \bar{n} , expressed in photon number units. Assume first that the relative phase between the signals is fixed. The receiver combines the signals on a balanced beam splitter. The time-integrated light intensity at the two output ports of the beam splitter labeled with indices ‘+’ and ‘−’ reads

$$I^\pm(\mathcal{V}) = \frac{\eta\bar{n}}{2}(1 \pm \text{Re}\mathcal{V}), \quad (1)$$

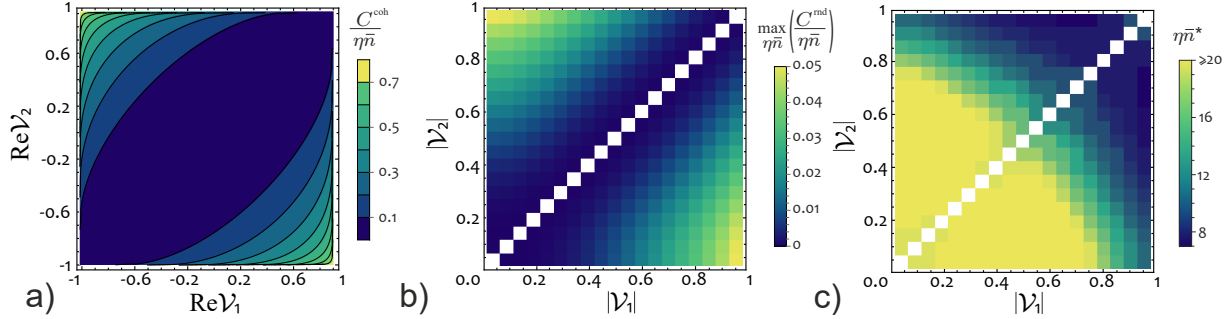


Figure 1. Discrimination between a pair of hypotheses encoded in interference visibilities $\mathcal{V}_1, \mathcal{V}_2$ for the coherent and the random-phase scenario. (a) Information gained from a single photodetection event for a fixed phase between interfering signals. (b) Maximum information per one detected photon $C^{\text{rnd}}/(\eta\bar{n})$ for signals with a random global phase. (c) Optimal $\eta\bar{n}^*$ maximizing the ratio $C^{\text{rnd}}/(\eta\bar{n})$. White squares on the diagonal in (b), (c) represent the case $|\mathcal{V}_1| = |\mathcal{V}_2|$ when the two hypotheses are indistinguishable.

where η is the channel transmission for each of the signals and \mathcal{V} is the interference visibility. As discussed in Appendix A, the visibility is proportional to the overlap between normalized mode functions describing the two signals. For identical signals with equal optical energies one has $\mathcal{V} = 1$ and completely destructive interference takes place at the ‘-’ output port. Let the output ports of the beam splitter be monitored by detectors that can resolve up to K photocounts over the signal duration. The probability p_k^\pm of registering k photocounts on one detector reads

$$p_k^\pm(\mathcal{V}) = \exp[-I^\pm(\mathcal{V})] \frac{[I^\pm(\mathcal{V})]^k}{k!} \quad (2)$$

for $k = 0, 1, \dots, K-1$ and $p_K^\pm(\mathcal{V}) = 1 - \sum_{k=0}^{K-1} p_k^\pm(\mathcal{V})$. Non-unit efficiency of the detectors can be included in the channel transmission η .

Suppose now that the signal pairs are received with a promise that the visibility takes only one of two equiprobable values \mathcal{V}_1 or \mathcal{V}_2 and that the interferometric measurement is repeated N times. The task is to discriminate between the two visibility hypotheses on the basis of the collected photocount sample. The probability ε of erroneously identifying the visibility can be upper bounded by the so-called Chernoff bound $\varepsilon \leq \exp(-NC)/2$ [14], where C stands for the Chernoff information given explicitly by

$$C = -\log \left[\min_{0 \leq \alpha \leq 1} \left(\sum_{k,k'=0}^K [P_{kk'}(\mathcal{V}_1)]^\alpha [P_{kk'}(\mathcal{V}_2)]^{1-\alpha} \right) \right]. \quad (3)$$

In the above expression, summation is carried out over all possible measurement outcomes, which in our setup have the form of two integers k and k' specifying the number of counts registered by individual

detectors, and $P_{kk'}(\mathcal{V})$ denotes the probability of obtaining a specific combination kk' for the visibility \mathcal{V} .

For the coherent signal scenario considered so far, the probability of registering respectively k and k' counts has the product form $P_{kk'}^{\text{coh}}(\mathcal{V}) = p_k^+(\mathcal{V})p_{k'}^-(\mathcal{V})$. Assuming full photon number resolution with $K \rightarrow \infty$, the Chernoff information can be simplified to

$$C^{\text{coh}} = \eta\bar{n} \left(1 - \frac{1}{2} \min_{0 \leq \alpha \leq 1} [(1 + \text{Re}\mathcal{V}_1)^\alpha (1 + \text{Re}\mathcal{V}_2)^{1-\alpha} + (1 - \text{Re}\mathcal{V}_1)^\alpha (1 - \text{Re}\mathcal{V}_2)^{1-\alpha}] \right). \quad (4)$$

It is seen that the Chernoff information is proportional to the received optical energy $\eta\bar{n}$. The proportionality factor given by the ratio $C^{\text{coh}}/(\eta\bar{n})$ can be interpreted as the amount of information gained from the detection of one photon. In Fig. 1(a) we depict this factor as a function of the real parts of visibilities $\text{Re}\mathcal{V}_1$ and $\text{Re}\mathcal{V}_2$. Generally, it pays off to maintain a large distance between the visibilities with the maximum information attained at $\mathcal{V}_1 = -\mathcal{V}_2 = \pm 1$. Note that in a realistic scenario the visibilities are reduced by inevitable imperfections, such as detector dark counts and misalignment of optical beams. A model including these effects is presented in Appendix A.

The above picture becomes much more nuanced if the sending parties have no access to a shared phase reference, which implies that the signals arrive with a random relative phase. However, in each individual realization the signals are described by coherent waveforms whose overlap is given by \mathcal{V} up to an overall phase factor. In such a scenario, the joint

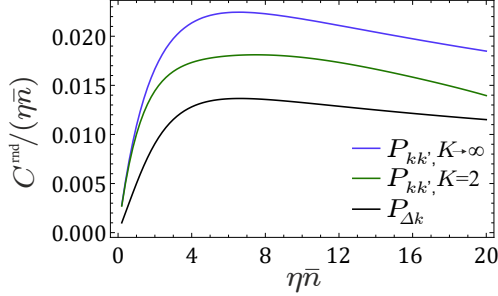


Figure 2. Information per one detected photon $C^{\text{rnd}}/(\eta\bar{n})$ as a function of the average photon number $\eta\bar{n}$ in a single realization of the visibility measurement with a random global phase, depicted for the pair of visibilities $\mathcal{V}_1 = 0.98$ and $\mathcal{V}_2 = 0.56$. The scenario of fully PNR detectors $K \rightarrow \infty$ (blue line) is compared with limited photon number resolution $K = 2$ (green line), and inference based only on the photocount difference $\Delta k = k' = k$ between two PNR detectors (black line).

photocount distribution reads

$$P_{kk'}^{\text{rnd}}(\mathcal{V}) = \int_0^{2\varphi} \frac{d\varphi}{2\pi} p_k^+(e^{i\varphi}\mathcal{V}) p_{k'}^-(e^{i\varphi}\mathcal{V}). \quad (5)$$

The explicit analytical expression for $P_{kk'}^{\text{rnd}}(\mathcal{V})$ is derived in Appendix B. Obviously, after averaging over the global phase only the absolute value $|\mathcal{V}|$ of the visibility parameter is relevant. The above probability distribution can be used to calculate the respective Chernoff information C^{rnd} according to Eq. (3). As before, the ratio $C^{\text{rnd}}/(\eta\bar{n})$ has the interpretation of the amount of information gained per one received photon.

In Fig. 2 we depict $C^{\text{rnd}}/(\eta\bar{n})$ as a function of the received optical energy $\eta\bar{n}$ for an exemplary pair of visibilities $\mathcal{V}_1 = 0.98$ and $\mathcal{V}_2 = 0.56$. The linear dependence of the ratio for $\eta\bar{n} \ll 1$ is explained by the fact that for very weak signals, detection of minimum two photons in a single realization of the measurement is necessary to obtain any meaningful information. Consequently, in this regime the leading term of the Chernoff information C^{rnd} is proportional to $(\eta\bar{n})^2$, which gives unfavorable quadratic scaling with the channel transmission. Beyond the two-photon regime corresponding to low optical energies, the ratio $C^{\text{rnd}}/(\eta\bar{n})$ exhibits a well pronounced maximum in $\eta\bar{n}$. This observation can be used to draw the following operational conclusion. Suppose that the total optical energy available at transmitters is \bar{n}_{tot} . If \bar{n} photons are used in a single realization of the interferometric measurement, one can afford $N = \bar{n}_{\text{tot}}/\bar{n}$ repetitions. Let us rewrite the Chernoff bound on the error probability as $\exp(-NC^{\text{rnd}})/2 = \exp[-\eta\bar{n}_{\text{tot}}C^{\text{rnd}}/(\eta\bar{n})]/2$. As-

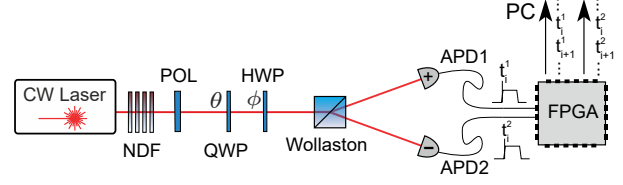


Figure 3. The simplified scheme of experimental setup. NDF, neutral density filters; POL, polariser; HWP, half-wave plate; QWP, quarter-wave plate; APD, avalanche photodiode; FPGA, time tapper based on field-programmable gate array.

suming a fixed \bar{n}_{tot} , which can be taken as the overall cost of implementing the communication primitive, it is beneficial to optimize $C^{\text{rnd}}/(\eta\bar{n})$ for a single realization.

Remarkably, the optimum of $C^{\text{rnd}}/(\eta\bar{n})$ occurs for $\eta\bar{n}$ in the few-photon range, which implies that PNR detectors are essential to acquire efficiently information needed for hypothesis testing. To illustrate this point, in Fig. 2 we depict also the noticeably lower ratio $C^{\text{rnd}}/(\eta\bar{n})$ calculated for detectors that can resolve only up to $K = 2$ photons. Importantly, the information about the actual visibility is distributed in a non-trivial manner across the entire joint photocount statistics. For example, using only the marginal distribution for the photocount number difference $P_{\Delta k}(\mathcal{V}) = \sum_k P_{k,k+\Delta k}(\mathcal{V})$ reduces significantly the Chernoff information, as also shown in Fig. 2. The above observations are universal as long as one of the two visibilities is sufficiently high, which is the case of quantum protocols motivating this study. In Fig. 1(b,c) we plot the maximum $C^{\text{rnd}}/(\eta\bar{n})$ as a function of the absolute values of the visibilities $|\mathcal{V}_1|$ and $|\mathcal{V}_2|$ to be discriminated between, along with the optimal average photon number that should be used in a single realization. Generally, the amount of information per unit optical energy is lower than in the coherent scenario depicted in Fig. 1(a), which is easily explained by the lack of the phase reference. Nevertheless, the available information also scales linearly with the optical energy, which implies that the scaling advantage over classical protocols should be analogous to the coherent case.

We performed a proof-of-principle experimental demonstration of binary hypothesis testing for a pair of visibilities $\mathcal{V}_1 = 0.98$ and $\mathcal{V}_2 = 0.56$ using a collinear interferometric setup presented in Fig. 3. We employed a continuous-wave 800 nm laser diode attenuated by a series of neutral-density filters down to $\approx 10^{-14}$ W of power followed by a polarizer ensuring a well-defined linear polarization. The beam is subsequently sent through a combination of a quarter- and a half-wave plate whose

respective rotation angles θ and ϕ define the normalized intensities after the Wollaston polarizer as $I^\pm = (1 \pm \text{Re}[e^{4i\phi - 2i\theta} \cos(2\theta)]) / 2$. Hence our experimental setup can be viewed as a fully equivalent simulation of a standard interferometer with the complex visibility tunable in the entire phase and absolute value range by an appropriate rotation of the wave plates. To realize the random phase scenario we collected the data for 50 half-wave plate angles ϕ uniformly probing a full period of the visibility phase. Both output beams were monitored by free-running avalanche photodiodes (APD) connected to a time tagger based on field-programmable gate array architecture, which registered photocounts with 3.3 ns temporal resolution.

The PNR detection was implemented using temporal domain multiplexing. We grouped time tagged counts for each of the two detectors over 80 μs -long time intervals. With the used input power, this interval corresponds to the mean photocount number $\eta\bar{n} = 6$ which gives the partitioning of the total optical energy that maximizes information per one detected photon. The numbers of photodetection events accumulated over an individual interval yield the single realization outcome kk' . The 50 ns dead time of the detectors used in the setup did not noticeably distort the measured photon statistics. We collected approx. 1.5×10^6 pairs kk' for each of the two visibilities. This allowed us to determine the joint probability distributions $P_{kk'}^{\text{rnd}}(\mathcal{V}_{1,2})$ depicted in Fig. 4(a), which within the resolution of the graphs match perfectly the theoretical values given by Eq. (5) (see Appendix B for a detailed discussion). For completeness, we show also in Fig. 4(b) experimentally determined marginal distribution for the photocount number difference $\Delta k = k' - k$.

In order to experimentally determine the error probability of binary hypothesis testing one needs to repeat the test procedure multiple times feeding it with independent sets of experimental data obtained for a fixed visibility. We realized this by selecting from the experimental results an ensemble of $M = 1.5 \times 10^4$ datasets $[(kk')_1, \dots, (kk')_N]_1, [(kk')_1, \dots, (kk')_N]_2, \dots, [(kk')_1, \dots, (kk')_N]_M$ consisting of N photocount pairs. We applied the Neyman-Pearson test [14] to each dataset deciding as a true one a visibility yielding a higher likelihood of photocounts group observation i.e. \mathcal{V}_1 if $\prod_{i=1}^N P_{(kk')_i}^{\text{rnd}}(\mathcal{V}_1) > \prod_{i=1}^N P_{(kk')_i}^{\text{rnd}}(\mathcal{V}_2)$ and \mathcal{V}_2 otherwise. The probability of error was evaluated as a ratio of erroneous hypothesis determinations to the number of groups M used for testing. We estimated the error for both visibilities which resulted in a pair of conditional errors $\varepsilon(\mathcal{V}_1|\mathcal{V}_2)$ and $\varepsilon(\mathcal{V}_2|\mathcal{V}_1)$, where $\varepsilon(\mathcal{V}|\mathcal{V}')$ denotes the probability of inferring visibility \mathcal{V} when \mathcal{V}' was the true one.

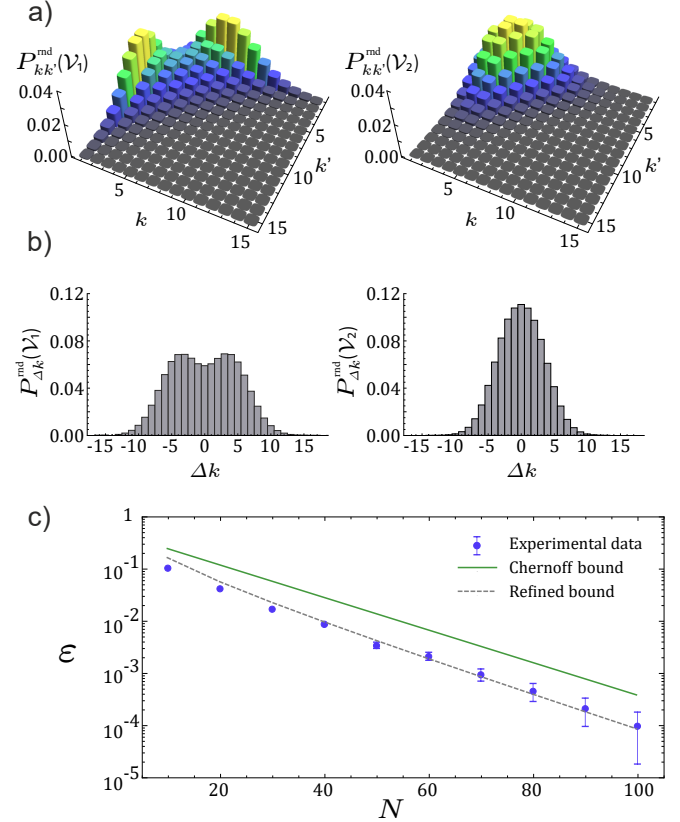


Figure 4. (a) Experimental joint photocount distributions $P_{kk'}^{\text{rnd}}$ obtained from approx. 1.5×10^6 outcomes kk' for visibilities $\mathcal{V}_1 = 0.98$ (left) $\mathcal{V}_2 = 0.56$ (right). (b) Marginal photocount difference distributions $P_{\Delta k}^{\text{rnd}}(\mathcal{V})$ for $\Delta k = k' - k$ (c) The error probability ε in hypothesis testing as a function of the dataset size N , determined for each N from 1.5×10^4 repetitions of the Neyman-Pearson test on independent sets of experimental data. The results are compared with the standard Chernoff bound (green, solid line) and its refined version (grey, dashed line). The errorbars account for one standard deviation.

In Fig. 4(c) we compare average error probability determined from experimental data $\varepsilon = [\varepsilon(\mathcal{V}_1|\mathcal{V}_2) + \varepsilon(\mathcal{V}_2|\mathcal{V}_1)] / 2$ with both the standard Chernoff bound for the random phase scenario and the refined Chernoff bound [15] (see Appendix C). According to theoretical predictions, the experimental error remains below the upper-bound provided by the Chernoff bound [14] reaching its refined version for asymptotically large number N of outcomes used for hypothesis testing [15]. Note that for big dataset sizes the error bars given by $\sqrt{\varepsilon(1-\varepsilon)/M}$ are of the order of the estimated probability of error. This is because ε becomes very small in this regime and is of the order of the inverse of the number of photocounts datasets M used for experimental error estimation.

In conclusion, we described and verified experimentally a strategy to identify the modal overlap between two optical signals with a random relative phase. The essential ingredient of the proposed approach is to utilize higher-order interference which modifies the joint photocount statistics at the interferometer output. When the identification task is formulated as binary hypothesis testing, the optimal way to utilize given optical energy is to repeat the visibility measurement multiple times in the few-photon regime. Such a measurement can be viewed as an implementation primitive for a number of quantum-enhanced protocols, when a shared phase reference is not available. Because its performance exhibits the same linear dependence the number of used photons as the scheme based on first-order coherence, one can expect a comparable quantum

advantage in scaling against classical protocols [13].

FUNDING INFORMATION

Foundation for Polish Science (TEAM/2016-1/1), M. J. was supported by the Foundation for Polish Science.

ACKNOWLEDGMENTS

We wish to acknowledge insightful discussions with E. Kashefi, N. Lütkenhaus, and Q. Zhang

See Supplement 1 for supporting content.

-
- [1] G. Brassard, “Quantum communication complexity,” *Foundations of Physics* **33**, 1593–1616 (2003).
- [2] H. Buhrman, R. Cleve, S. Massar, and R. de Wolf, “Nonlocality and communication complexity,” *Rev. Mod. Phys.* **82**, 665–698 (2010).
- [3] D. Gottesman and I. Chuang, “Quantum digital signatures,” arXiv:quant-ph/1015032 (2001).
- [4] H. Buhrman, R. Cleve, J. Watrous, and R. de Wolf, “Quantum fingerprinting,” *Phys. Rev. Lett.* **87**, 167902 (2001).
- [5] J. M. Arrazola and N. Lütkenhaus, “Quantum fingerprinting with coherent states and a constant mean number of photons,” *Phys. Rev. A* **89**, 062305 (2014).
- [6] J. M. Arrazola and N. Lütkenhaus, “Quantum communication with coherent states and linear optics,” *Phys. Rev. A* **90**, 042335 (2014).
- [7] P. L. Clarke, R. Collins, V. Dunjko, E. Andersson, J. Jeffers, and G. S. Buller, “Experimental demonstration of quantum digital signatures using phase-encoded coherent states of light,” *Nat. Commun.* **3**, 1174 (2012).
- [8] R. J. Collins, R. J. Donaldson, V. Dunjko, P. Wallden, P. J. Clarke, E. Andersson, J. Jeffers, and G. S. Buller, “Realization of quantum digital signatures without the requirement of quantum memory,” *Phys. Rev. Lett.* **113**, 040502 (2014).
- [9] F. Xu, J. M. Arrazola, K. Wei, W. Wang, P. Palacios-Avila, C. Feng, S. Sajeed, N. Lütkenhaus, and H. K. Lo, “Experimental quantum fingerprinting with weak coherent pulses,” *Nat. Commun.* **6**, 8735 (2015).
- [10] J.-Y. Guan, F. Xu, H.-L. Yin, Y. Li, W.-J. Zhang, S.-J. Chen, X.-Y. Yang, L. Li, L.-X. You, T.-Y. Chen, Z. Wang, Q. Zhang, and J.-W. Pan, “Observation of quantum fingerprinting beating the classical limit,” *Phys. Rev. Lett.* **116**, 240502 (2016).
- [11] R. T. Horn, S. A. Babichev, K.-P. Marzlin, A. I. Lvovsky, and B. C. Sanders, “Single-qubit optical quantum fingerprinting,” *Phys. Rev. Lett.* **95**, 150502 (2005).
- [12] J. Du, P. Zou, X. Peng, D. K. L. Oi, L. C. Kwek, C. H. Oh, and A. Ekert, “Experimental quantum multimeter and one-qubit fingerprinting,” *Phys. Rev. A* **74**, 042319 (2006).
- [13] M. Jachura, M. Lipka, M. Jarzyna, and K. Banaszek, “Quantum fingerprinting using two-photon interference,” arXiv:quant-ph/1710.02336 (2017).
- [14] T. M. Cover and J. A. Thomas, *Elements of Information Theory* (Wiley, 1991).
- [15] R. R. Bahadur and R. R. Rao, “On deviations of the sample mean,” *Ann. Math. Statist.* **31**, 1015–1027 (1960).

Visibility-based hypothesis testing using higher-order optical interference: supplementary material

This document provides supplementary information to "Visibility-based hypothesis testing using higher-order optical interference". We present here derivation of the interference visibility of light in two partially overlapping modes and show how dark counts can be incorporated into the effective visibility. We also derive an analytic expression for photocounts probability in the random phase scenario and compare it with experimentally measured statistics. Finally, we derive a refined Chernoff bound for the error probability in binary hypothesis testing.

Appendix A: Interference visibility

Consider two optical signals with amplitudes α and β , described by normalized complex waveforms in the temporal domain $u(t)$ and $v(t)$,

$$\int dt |u(t)|^2 = \int dt |v(t)|^2 = 1. \quad (\text{A1})$$

The signals are combined at a balanced beam splitter. The time-integrated intensities at the output ports of the beam splitter can be written as:

$$\begin{aligned} I_{\pm} &= \frac{1}{2} \int dt |\alpha u(t) \pm \beta v(t)|^2 \\ &= \frac{|\alpha|^2 + |\beta|^2}{2} \left[1 \pm \text{Re} \left(\frac{2\alpha^*\beta}{|\alpha|^2 + |\beta|^2} \int dt u^*(t)v(t) \right) \right] \end{aligned} \quad (\text{A2})$$

This expression has the form given by Eq. (1) in the main text with $|\alpha|^2 + |\beta|^2 = \eta\bar{n}$ and

$$\mathcal{V} = \frac{2\alpha^*\beta}{|\alpha|^2 + |\beta|^2} \int dt u^*(t)v(t). \quad (\text{A3})$$

When the signals have equal amplitudes, $\alpha = \beta$, the visibility parameter \mathcal{V} is given directly by the scalar product between the normalized signal waveforms. If the signals are misaligned at the beam splitter, e.g. in the transverse spatial degree of freedom, \mathcal{V} is additionally multiplied by a spatial integral characterizing the overlap between spatial field distributions.

If the detectors employed to determine the photocount statistics exhibit dark counts characterized by Poissonian statistics with the mean \bar{n}_{dark} over the measurement time, the time integrated intensities in Eq. (A2) need to be replaced by $I_{\pm} \rightarrow I_{\pm} + \bar{n}_{\text{dark}}$. It is straightforward to show that in this scenario they can also be cast into the form given by the right hand side of Eq. (1) with the following substitutions:

$$\begin{aligned} \eta\bar{n} &\rightarrow \eta\bar{n} + 2\bar{n}_{\text{dark}} \\ \mathcal{V} &\rightarrow \frac{\eta\bar{n}}{\eta\bar{n} + 2\bar{n}_{\text{dark}}} \mathcal{V}. \end{aligned} \quad (\text{A4})$$

Thus the effective visibility is reduced by the factor $\eta\bar{n}/(\eta\bar{n} + 2\bar{n}_{\text{dark}})$.

Appendix B: Experimental vs Theoretical joint photocounts distribution

Below we shall derive the explicit expression for theoretical phase-averaged distribution of joint photocounts $P_{kk'}^{\text{rnd}}(\mathcal{V})$ as well present its quantitative comparison with experimental data.

Let us begin with the formula describing the output intensities I^{\pm} for the visibility $\mathcal{V} = e^{i\varphi}|\mathcal{V}|$

$$I^{\pm}(\mathcal{V}) = \frac{\eta\bar{n}}{2}(1 + |\mathcal{V}| \cos \varphi) \quad (\text{B1})$$

The phase-averaged distribution is given by the integral:

$$P_{kk'}^{\text{rnd}}(\mathcal{V}) = \int_0^{2\varphi} \frac{d\varphi}{2\pi} p_k^+(e^{i\varphi}\mathcal{V}) p_{k'}^-(e^{i\varphi}\mathcal{V}). \quad (\text{B2})$$

Since the count statistics on one photodetector is given by a Poissonian distribution $p_k^{\pm}(\mathcal{V}) = \exp[-I^{\pm}(\mathcal{V})][I^{\pm}(\mathcal{V})]^k/k!$ the joint phase-averaged distribution can be expressed as:

$$P_{kk'}^{\text{rnd}}(\mathcal{V}) = \int_0^{2\varphi} \frac{d\varphi}{2\pi} \frac{1}{k!k'!} [I^+(\mathcal{V})]^k [I^-(\mathcal{V})]^{k'} e^{-I^+(\mathcal{V})-I^-(\mathcal{V})}. \quad (\text{B3})$$

After plugging the explicit formulas for the intensities (B1) into the integrand, the RHS of Eq. B3 becomes:

$$\frac{e^{-\eta\bar{n}}(\eta\bar{n})^{k+k'}}{2^{k+k'}k!k'!} \int_0^{2\varphi} \frac{d\varphi}{2\pi} (1+|\mathcal{V}| \cos \varphi)^k (1-|\mathcal{V}| \cos \varphi)^{k'}, \quad (\text{B4})$$

which after applying binomial expansions can be written as:

$$\frac{e^{-\eta\bar{n}}(\eta\bar{n})^{k+k'}}{2^{k+k'}k!k'!} \int_0^{2\varphi} \frac{d\varphi}{2\pi} \sum_{m=0}^k \sum_{n=0}^{k'} \binom{k}{m} \binom{k'}{n} (-1)^n |\mathcal{V}|^{m+n} (\cos \varphi)^{m+n}. \quad (\text{B5})$$

We can simplify the expression by reordering the integral and the double-sum:

$$P_{kk'}^{\text{rnd}}(\mathcal{V}) = \sum_{m=0}^k \sum_{n=0}^{k'} \frac{e^{-\eta\bar{n}}(\eta\bar{n})^{k+k'} (-1)^n |\mathcal{V}|^{m+n}}{2^{k+k'} m!(k-m)!n!(k'-n)!} \int_0^{2\varphi} \frac{d\varphi}{2\pi} (\cos \varphi)^{m+n}, \quad (\text{B6})$$

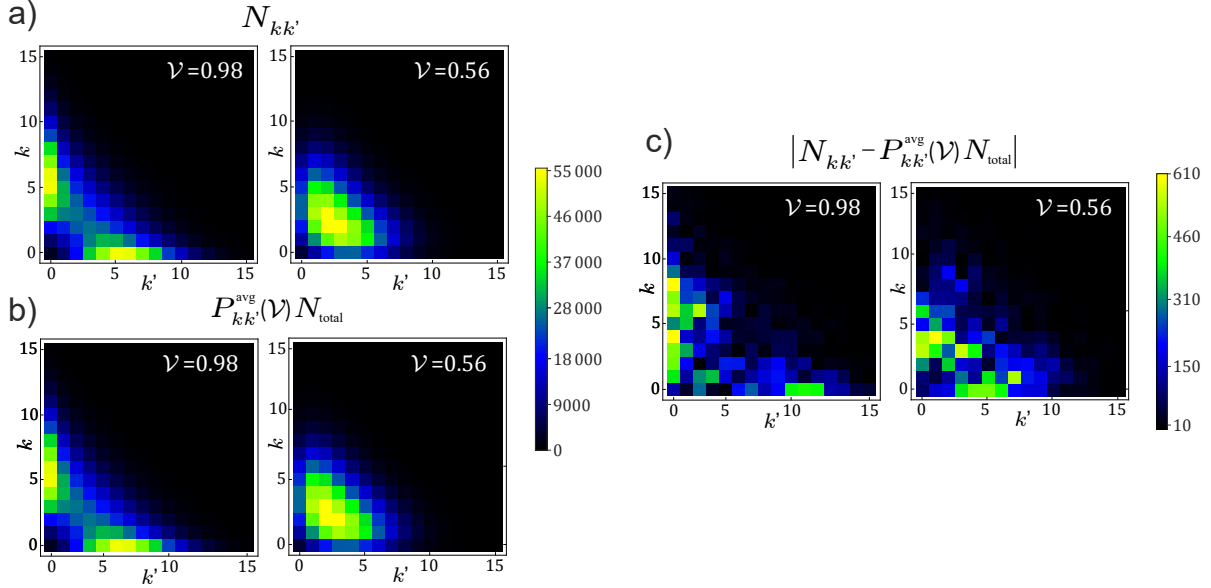


Figure 5. Comparison between experimentally measured statistics of photocounts $N_{kk'}$ (a) and theoretically predicted distributions given by $P_{kk'}^{\text{rnd}}(\mathcal{V})N_{\text{total}}$ (b), where $N_{\text{total}} = \sum_{k,k'=0}^{15} N_{kk'}$ and $P_{kk'}^{\text{rnd}}(\mathcal{V})$ is defined in Eq. B6. The point-to-point difference between experimental statistics and the theoretical distribution presented in (c) does not exceed measurement uncertainty.

The phase-averaged integer powers of cosine function can be calculated analytically yielding a compact solution:

$$\int_0^{2\varphi} \frac{d\varphi}{2\pi} (\cos \varphi)^j = \begin{cases} 0 & \text{odd } j \\ \frac{1}{2^j} \binom{j}{j/2} & \text{even } j, \end{cases}$$

which makes Eq. (B6) simple enough to evaluate using symbolic computation programs such as Wolfram Mathematica.

In a realistic scenario the joint photocounts distribution is truncated due to the finite resolution of PNR detectors of up to K photocounts. Since all possible pairs kk' with single or both photocounts exceeding the PNR resolution, contribute to marginal values $P_{Kk'}$, P_{kK} or P_{KK} , the measured distribution $P_{kk'}(\mathcal{V})$ is composed of four expressions:

$$P_{kk'}(\mathcal{V}) = \begin{cases} P_{kk'}^{\text{rnd}}(\mathcal{V}) & k, k' < K \\ \sum_{k'=K}^{\infty} P_{kk'}^{\text{rnd}}(\mathcal{V}) & k < K, k' = K \\ \sum_{k=K}^{\infty} P_{kk'}^{\text{rnd}}(\mathcal{V}) & k' < K, k = K \\ \sum_{k,k'=K}^{\infty} P_{kk'}^{\text{rnd}}(\mathcal{V}) & k' = K, k = K, \end{cases}$$

such that $\sum_{k,k'=0}^K P_{kk'}(\mathcal{V}) = 1$. To avoid the information loss resulting from the distribution truncation we carefully adjusted the beam intensity and counts grouping time to resolve virtually all possible photocounts.

In Fig. S1 we present a comparison between experimentally measured numbers $N_{kk'}$ of observed photocount pairs kk' Fig. S1(a) and the theoretical prediction given by $P_{kk'}^{\text{rnd}}(\mathcal{V})N_{\text{total}}$ Fig. S1(b), where $N_{\text{total}} = \sum_{k,k'=0}^{15} N_{kk'}$ stands for the total number of registered pairs. The point-to-point difference between experimental statistics and the theoretical distribution presented in Fig. S1(c) does not generally exceed two standard deviations of measured counts number given by $\sqrt{N_{kk'}}$.

Appendix C: Refined Chernoff bound

Here we will present a derivation of a refined version of the Chernoff bound following [15]. Assume that we want to distinguish between two equiprobable hypotheses, characterized by random distributions $p(x)$ and $q(x)$, based on N repetitions of the experiment in a way that minimizes the average error. If we perform Neyman-Pearson test [14] we choose as the correct one the hypothesis that yields larger likelihood. The average probability of error is then given by

$$\varepsilon = \frac{1}{2} (\Pr[p(x_1) \dots p(x_N) \geq q(x_1) \dots q(x_N)|q] + \Pr[q(x_1) \dots q(x_N) \geq p(x_1) \dots p(x_N)|p]), \quad (\text{C1})$$

where $\Pr[q(x_1)\dots q(x_N) \geq p(x_1)\dots p(x_N)|p]$ denotes the probability that we will obtain values x_1, \dots, x_N for which $q(x_1)\dots q(x_N) \geq p(x_1)\dots p(x_N)$ assuming the correct hypothesis is given by $p(x)$, and analogously for $\Pr[p(x_1)\dots p(x_N) \geq q(x_1)\dots q(x_N)|q]$. Let us consider the first probability, i.e. $\Pr[q(x_1)\dots q(x_N) \geq p(x_1)\dots p(x_N)|p]$. We may take the condition $q(x_1)\dots q(x_N) \geq p(x_1)\dots p(x_N)$ and divide both sides by the right hand side

$$\frac{p(x_1)}{q(x_1)} \dots \frac{p(x_N)}{q(x_N)} \leq 1, \quad (\text{C2})$$

which after taking a natural logarithm and dividing by N translates into

$$\frac{1}{N} \left(\log \frac{p(x_1)}{q(x_1)} + \dots + \log \frac{p(x_N)}{q(x_N)} \right) \leq 0. \quad (\text{C3})$$

Let us introduce a new random variable $y = f(x) = -\log \frac{p(x)}{q(x)}$. Since x is distributed according to $p(x)$, y is distributed according to an induced probability distribution $P_y(y) = p(f^{-1}(y))$. The moment generating function of y is given by

$$\begin{aligned} \varphi_y(t) &= \sum_y e^{ty} P_y(y) = \sum_y e^{ty} p(f^{-1}(y)) = \\ &= \sum_x q(x)^t p(x)^{1-t}. \end{aligned} \quad (\text{C4})$$

We may now write Eq. (C3) as a condition for the mean value of y

$$\frac{1}{N} \sum_{i=1}^N y_i \geq 0. \quad (\text{C5})$$

According to [15] the probability that a mean value is larger than 0 can be written as

$$\Pr \left(\frac{y_1 + \dots + y_N}{N} \geq 0 \right) = \rho^N \left(\frac{1}{\sqrt{2\pi N} \gamma} + O(N^{-3/2}) \right), \quad (\text{C6})$$

where $\rho = \varphi_y(\tau)$ and $\gamma = \sigma\tau$, where $\sigma^2 = \varphi_y''(\tau)/\varphi_y(\tau)$ and τ is defined implicitly by the equation $\varphi_y'(\tau)/\varphi_y(\tau) = 0$. Using Eq. (C4) we may rewrite the definition of τ as

$$\begin{aligned} \frac{\varphi_y'(\tau)}{\varphi_y(\tau)} &= \sum_x p^*(x) \log \frac{q(x)}{p(x)} = \\ &= \sum_x p^*(x) [\log q(x) - \log p^*(x) + \log p^*(x) - \log p(x)] = \\ &= D(p^*||p) - D(p^*||q) = 0, \end{aligned} \quad (\text{C7})$$

where $p^*(x) = p(x)^{1-\tau} q(x)^\tau / (\sum_x p(x)^{1-\tau} q(x)^\tau)$ and $D(p||q) = \sum_x p(x) \log \frac{p(x)}{q(x)}$ is the relative entropy. The solution to the above equation is given by the coefficient $\tau = \alpha^*$ optimizing the Chernoff information $C = \min_{0 \leq \alpha \leq 1} \log \sum_x q(x)^\alpha p(x)^{1-\alpha}$ [14]. Using this result, other quantities required in Eq. (C6) are given by

$$\rho = e^{-C}, \quad \sigma^2 = \sum_x p^*(x) \left(\log \frac{p(x)}{q(x)} \right)^2 \quad (\text{C8})$$

Repeating calculations for the second probability, $\Pr[q(x_1)\dots q(x_N) \geq p(x_1)\dots p(x_N)|p]$, and adding the results we eventually obtain a refined bound on the average error probability

$$\varepsilon = \frac{1}{\sqrt{2\pi N}} \frac{e^{-NC}}{2\alpha^*(1-\alpha^*)\sigma}. \quad (\text{C9})$$